Fast spiking interneuron activity in primate striatum tracks learning of attention cues

Kianoush Banaie Boroujeni[a], Mariann Oemisch[b,c], Seyed Alireza Hassani[a], and Thilo Womelsdorf[a,b,1]

[a]Department of Psychology, Vanderbilt University, Nashville, TN 37240; [b]Department of Biology, Centre for Vision Research, York University, Toronto, ON M6J 1P3, Canada; and [c]Zanvyl Krieger Mind/Brain Institute, Johns Hopkins University, Baltimore, MD 21218

Cognitive flexibility depends on a fast neural learning mechanism for enhancing momentary relevant over irrelevant information. A possible neural mechanism realizing this enhancement uses fast spiking interneurons (FSIs) in the striatum to train striatal projection neurons to gate relevant and suppress distracting cortical inputs. We found support for such a mechanism in nonhuman primates during the flexible adjustment of visual attention in a reversal learning task. FSI activity was modulated by visual attention cues during feature-based learning. One FSI subpopulation showed stronger activation during learning, while another FSI subpopulation showed response suppression after learning, which could indicate a disinhibitory effect on the local circuit. Additionally, FSIs that showed response suppression to learned attention cues were activated by salient distractor events, suggesting they contribute to suppressing bottom-up distraction. These findings suggest that striatal fast spiking interneurons play an important role when cues are learned that redirect attention away from previously relevant to newly relevant visual information. This cue-specific activity was independent of motor-related activity and thus tracked specifically the learning of reward predictive visual features.

cognitive flexibility | reversal learning | reinforcement learning | confidence | caudate nucleus

Adaptive behavior depends on neural mechanisms that enhance the processing of momentary relevant information and disengage from processing irrelevant information. Both these adaptive processes are believed to depend on the anterior striatum (1–3). One reason for this alleged role of the striatum to adjust behavior flexibly is its rich and diverse input from brain areas that represent the current behavioral goals, the values of recently experienced outcomes, and the reward value of available objects in the environment (4, 5). These inputs carry the information needed to decide whether ongoing cognitive routines are aligned to the current goal or whether they need to be adjusted. These diverse types of information are integrated in the striatum where neurons are observed that activate preferably to those inputs that are momentarily reward relevant (1, 4). This increase in activity to only a selected subset of the available visual information can be described as the gating of cortico-striatal inputs. How such a facilitation of inputs is achieved and what types of representations are supported by such a selective striatal activation are two fundamental questions that need to be solved to understand the neural basis of cognitive flexibility. Here, we address both of these questions.

Previous studies suggest that the synaptic integration of inputs in the striatum depends critically on fast spiking interneurons (FSIs) (6, 7). FSIs receive prominent inputs from cortical sources and impose feedforward inhibition on large ensembles of spiny projection neurons (SPNs) (8–11). This FSI-mediated inhibition has therefore been implicated to control how glutamatergic inputs from prefrontal cortices are gated to SPNs (12, 13). Recent in vivo evidence in rodent striatum supports this view by suggesting that the activation of SPNs to prefrontal inputs is modified by inhibition from FSIs during learning (12, 14, 15). According to

these insights it is possible that cognitive flexibility is supported by selective FSI-mediated inhibition during the flexible adjustment of behavior. This scenario predicts that FSI-mediated inhibition should be particularly strong during flexible cognitive adjustment in order to either prevent activation of SPNs that responded to previously relevant cues or to facilitate via disinhibition the activation of SPNs that respond to newly relevant cues. The consequence of such an inhibitory influence during learning would thus be the formation of a new assembly of cells becoming active after, as compared to before, learning (16).

Which type of information is processed in striatal cell assemblies? A hallmark of cognitive flexibility is that it operates on cognitive information independent of immediate motor requirements. Support for striatal processing of such "cognitive events" (4) comes from nonhuman primate studies about the efficient learning of values of unique objects in the anterior striatum (17–24). Striatal neurons fire stronger when objects appear at recently rewarded locations (18, 24, 25), and when attention is directed to the rewarded and away from nonrewarded stimuli (26). These activity changes indicate that striatal circuits might gate visual inputs for making choices (1, 23). Consistent with this view, electrical stimulation of primate anterior striatum can alter choices to stimuli that are associated with reward and that are part of specific stimulus-response mappings (25, 27–29), complementing optogenetic stimulation-induced changes in choice behavior reported in rodents (30–32). The stimulation-induced changes in choice behavior can be specific to visual objects irrespective of object locations or motor plans used to choose among objects (25). Taken together, these studies suggest that neural circuits in the striatum can operate on specific visual cues, opening the possibility

Significance

Cognitive flexibility entails the ability to disengage attention from stimuli when they fail to predict positive outcomes, and to engage attention to newly rewarding stimuli. This reconfiguration of attention is likely supported by neural circuits that assign values to visual features. We report that activity of two separable groups of fast spiking striatal interneurons are likely part of that neural circuit. We electrophysiologically identified distinct cell populations in the primate striatum and found that fast spiking interneurons changed their firing specifically at the onset of an attention cue during learning. These findings provide evidence for a role of fast spiking striatal neurons to mediate the flexible reconfiguration of attentional priorities during learning.

NEUROSCIENCE

that cue-triggered striatal routing is learned quickly in support of cognitive flexibility.

Here, we address these open questions about the learning of striatal gating by recording from striatal neurons in nonhuman primates during a feature-based reversal learning task. We first set out to establish a cell classification protocol that identifies FSIs in the striatum of nonhuman primates and distinguishes them from other local interneurons and from SPNs. We then quantified how the striatal cell types change their firing during reversal learning in response to visual cues that either instruct subjects to covertly shift attention or to overtly plan a saccadic eye movement. We found that two distinct FSI cell types can be reliably distinguished by their electrophysiological profiles. Both FSI cell types responded preferentially to the attention cue and both showed the strongest firing rate correlations with successful reversal learning compared to SPNs and other interneurons. These findings suggest that striatal FSIs play a role in learning the reward predicting value of visual cues that redirect attention away from previously relevant to newly relevant visual information.

Results

We used a color-based reversal paradigm that required subjects to learn the reward value of colors assigned to two stimuli. The color value remained constant for blocks of at least 30 trials before uncued reversals (Fig. 1*A*). Each trial involved the stepwise addition of informative features, serving as cues, to two initially identical gabor patches. During each trial the onset of color served as the attention color cue for shifting covert attention to the stimulus with the rewarded color, while an action motion cue was shown before or after the attention cue to associate a saccade direction (up- or downward) with the selection of each stimulus (Fig. 1*B*). After both cues were shown, the animals had to detect a go-signal (a transient dimming) in the stimulus with the rewarded color to make a saccade for obtaining the reward. A transient dimming occurred in one-third of the trials in the stimulus with the nonrewarded color prior to a dimming of stimulus with the rewarded stimulus, in which case it needed to be ignored (*SI Appendix*). The transient dimming of the nonrewarded stimulus thus reflected a no-go event because it instructed to inhibit responding. Monkeys learned the newly rewarded target object in each reversal block within 11 (SE: 2) trials showing learning curves that separated a learning period from a learned period with asymptotic probability for making rewarded choices (Fig. 1*C*). The reversal learning performance was well accounted for by a model-free reinforcement learning model augmented with a mechanism that enhances the speed of adjusting reward values for attended over nonattended (nonchosen) stimuli (23, 33) (*SI Appendix*).

Firing Patterns and Synchronization Distinguishes Fast Spiking Interneurons. While animals performed reversal learning, we recorded from 350 neurons in the anterior striatum of two monkeys (164/186 in monkeys K/H, Fig. 1*D*). Neurons fell into three separate action potential classes showing broad spikes (B, 83% [292 of 350]), medium spikes (M, 8% [28 of 350]), and narrow spikes (N, 9% [30 of 350]) (Fig. 2*A*) (three-Gaussian model, $P <$ 0.01, *SI Appendix*, Fig. S1 *A–C*). This tripartite split is similar to prior studies in rodent striatum showing that SPNs and FSIs have broad and narrow spikes, respectively (34–36). FSIs and SPNs are also distinguished by how bursty and regular their firing is (6), which we quantified using their spiketrains' local variability (LV) (37) and global variability (coefficient of variation [CV]) (*SI Appendix*, Fig. S1 *D* and *E*). We combined these firing parameters with the action potential parameters (rise and decay times) for improving the separation of FSIs using cluster analysis. We found that firing patterns and action potentials explained 93.9% of the dataset variance and distinguished two narrow spiking cell classes (N1 and N2), four broad spiking cell classes (B1 to B4), and a class

with medium action potential width (M1) (Fig. 2 *B* and *C* and *SI Appendix*, Fig. S1 *F* and *G*). The classes were composed of 29, 8, and 18 cells for N1, N2, and M1 cells, and 67, 62, 76, and 90, for B1 to B4 cells, respectively. Inspection of the spike rasters (Fig. 2*C*) and spike parameters suggested apparent mappings of these cell classes to classes defined using molecular tools and morphology variables. N2 and M1 fulfill criteria of FSIs by showing high firing rates and repetitive interspike intervals (LVs significantly smaller than 1, random permutation test, $P < 0.01$, *SI Appendix*, Fig. S1*H*). Low firing rates and narrow spikes associate the N1 class with cells that might include inhibitory low threshold spiking cells (LTS). The broad spiking classes B1 to B4 are likely dominated by SPNs, while among these B classes, B1 and B4 will likely include subsets of cholinergic interneurons and neurogliaform cells (see *Discussion*).

In addition to class-specific firing patterns, cell classes showed unique oscillatory sidelobes in spike-triggered local field potential (LFP) averages that indicated they synchronized differently to local striatal field potentials (*SI Appendix*, Fig. S2). Across the whole cell population, we found that cells synchronized significantly to either theta (4.5 ± 3 Hz), beta (16 ± 8 Hz), or gamma (38 ± 10 Hz) frequencies as evident in three peaks of a peak density histogram calculated across all spike-LFP pairs (Fig. 2*D*). The FSI classes (N2 and M1) showed a peak density indexing gamma band synchronization, but no beta frequency synchrony peaks, while the SPN-associated classes B2 to B4 showed synchronization peak densities in the beta frequency band (Fig. 2*E*). Classes B1 and B2 were broad spiking classes with a gamma peak similar to the narrow spiking cells. Using support vector machine classification, we could predict significantly more likely than chance the class label of cells from the cells' strength of spike-LFP synchronization (*SI Appendix*, Fig. S2*C*). This finding showed that putative SPN classes showed class-specific beta band synchrony, while putative FSI classes M1 and N2 showed gamma synchrony consistent with evidence from the rodent striatum (34, 38, 39).

Fast Spiking Interneuron Responses to Attention and Action Cues. Distinguishing FSIs (M1 and N2) from SPN-dominated cell classes allowed us to test how these classes responded to the attention cue onset. We found in multiple examples that striatal neurons responded strongly to the onset of the attention color cue, regardless of whether it appeared before or after the action (motion) cue during a trial (Fig. 3*A*, for more examples, see *SI Appendix*, Fig. S3). Across the population, a majority of striatal neurons showed maximal firing rate modulations in the 0.4 s after attention cue onset (Fig. 3*B*), while response modulations to the action motion cue were rarer and less pronounced (Fig. 3*C*). This attention cue-specific responding varied between cell classes. One FSI class (N2, $n = 8$ cells included in this analysis) showed a significant, fast, and transient on-response to the attention cue (Fig. 3*D*, $P < 0.05$ increase from 0 to 0.1 s after cue onset, random permutation test), that was not evident for the action cue (Fig. 3*E*). When N2 cells ceased firing, cells of the B2 ($n = 25$ cells), B4 ($n = 10$ cells), and N1 ($n = 7$ cells) classes began to show increased firing to the attention cue ($P < 0.05$), but not to the action cue (Fig. 3*D*). In contrast to these firing increases, fast spiking M1 interneurons ($n = 13$ cells) reduced their firing to the attention cue (Fig. 3*D*, $P <$ 0.05 decrease from 0.2 s after cue onset onwards, random permutation test). Direct comparison of attention cue versus action cue onset responses confirmed that N1, N2, M1, B2, and B4 showed stronger modulations to the attention cue than the action cue onset (Fig. 3*E*). These cell-specific attention cue responses were seen irrespective of whether the rewarded stimulus was ipsi- or contralateral to the recorded hemisphere (Fig. 3*F*).

Fast Spiking Interneuron Cue Responses Change with Reversal Learning. We next tested how the attention cue responses varied with the reversal learning of color values. We estimated the

www.manaraa.com
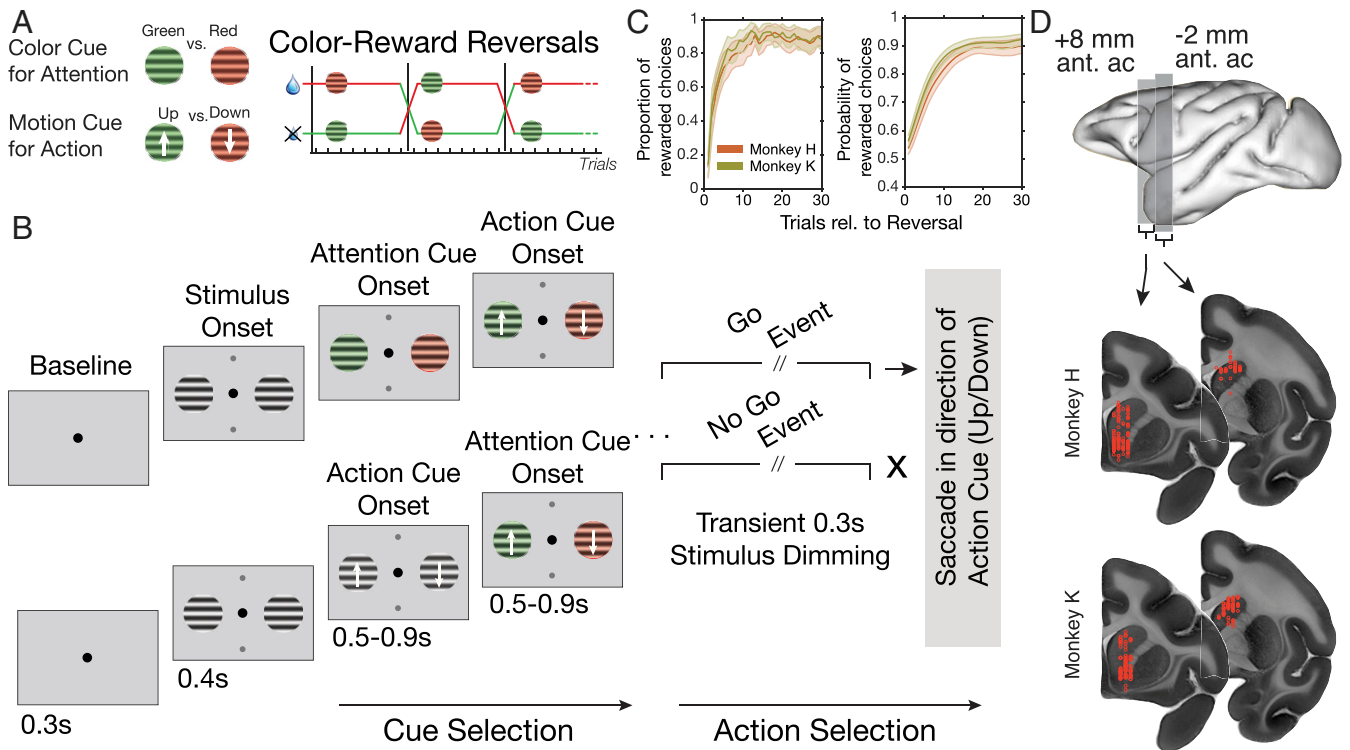
Fig. 1. Task paradigm. (*A*) The animals performed a color-based attentional learning task requiring learning to attend to the stimulus with the rewarded color and make a saccade in the direction of the motion of that stimulus. The color cue for attention and the motion cue for (saccadic) action varied independently from one another. Learning which color is rewarded proceeded in blocks of 30 trials before uncued color-reward reversals could happen. (*B*) During a trial, animals fixated the center dot and were shown the attention color cue or the action motion cue first. After 0.5 to 0.9 s the remaining cue was shown. Each stimulus could then transiently dim. The dimming was either in the target stimulus first, the distractor stimulus first, or in both stimuli simultaneously. The animal could make a saccade in the 0.05 to 0.55 s after dimming to receive feedback (reward or no reward). Since only one stimulus was rewarded per trial a dimming event was either a go cue to make a saccadic eye movement when it occurred in the rewarded stimulus, or it was a no-go cue for withholding a movement when it occurred in the nonrewarded stimulus. (*C*) Both monkeys learned the color-reversal task reaching ~85% plateau performance (*Left*). We estimated the learning status of the animals with an ideal observer statistic as probability to observe rewarded choice (*Right*). (*D*) Recording locations in the anterior striatum for monkeys H and K.

learning progress as the increased probability of subjects to make rewarded choices, which we refer to as the learning status (LS) (Fig. 1*C*) and used as learning criterion the trial when the lower confidence bound of the probability surpassed the chance level (40, 41). First, we found that the average firing prior to reaching the learning criterion tended to be larger for most cell classes for the attention cue epoch but not the action cue epoch (*SI Appendix*, Fig. S4 *A* and *B*). To quantify this effect, we correlated for each cell the postcue firing rates with the LS. Neurons with significant LS × rate correlations show rate modulations that vary with improved color-reward learning. Such a correlation is shown in an example cell in Fig. 4*A* that gradually reduced firing as the animal learned the new color rule. Across the striatum we found that the narrow spiking neurons (M1, N1, and N2) compared to broad spiking neurons (B1 to B4) were more likely to show significant LS × rate correlations (38% vs. 22%, $P < 0.01$, χ^2 test), showed stronger absolute average correlations with learning ($r = 0.19$ vs. $r = 0.09$, $P < 0.001$, bootstrap randomization test), and showed on average significantly negative correlations ($r = −0.10$ vs. $r = 0.00$, $P < 0.001$, bootstrap randomization test) (*SI Appendix*, Fig. S4*C*). Narrow spiking cells (M1, N1, and N2) were more likely to fire stronger early during learning or were suppressed after learning had occurred (stronger firing early during learning: seven cells; suppressed firing after learning: eight cells). Among these narrow spiking classes, it was particularly the fast spiking neuron classes M1 and N2 that showed significantly stronger and on average negative correlations of their firing rate

with learning status compared to other classes (M1: $r = −0.12$, $n = 10$; N1: $r = −0.05$, $n = 5$; N2: $r = −0.17$, $n = 7$; B1: $r = 0$, $n = 31$; B2: $r = 0.03$, $n = 24$; B3: $r = 0.01$, $n = 3$; B4: $r = 0.05$, $n = 8$) (Fig. 4*D*). Neurons of the M1 and N2 classes were the only classes that showed on average negative correlations of their firing rate with learning status, indicating strongest cue-triggered activity during learning (class N2), or reduced cue-triggered activity after learning (class M1) (Fig. 4*D*).

The correlation results so far were between firing rates and an ideal observer estimate of the probability of rewarded choices during reversal learning that can be interpreted as quantifying how confident a subject is that a specific color leads to reward (40). Concomitant to increased confidence about which color is relevant, reversal learning is also accompanied by increases in choice probability and expected = value for the relevant stimulus (Fig. 4*B*), raising the question as to which of these learning variables best correlate with neural firing. We estimated choice probability (CP) and the expected stimulus value (EV) with a reinforcement learning model (*SI Appendix*) and performed partial correlations of firing rates with learning status, CP, and EV for narrow and broad spiking cells (cells in the analysis: narrow = 21, and broad = 65). We found that the ideal observer-estimated confidence was significantly more likely correlated with the firing of narrow than broad spiking neurons (48%, $n = 10$, of narrow and 14%, $n = 9$, for broad spiking neurons), and was on average significantly negatively correlated with the firing of narrow spiking neurons ($r = −0.07$ for narrow and $r = 0.003$ for

Banaie Boroujeni et al.

www.manaraa.com
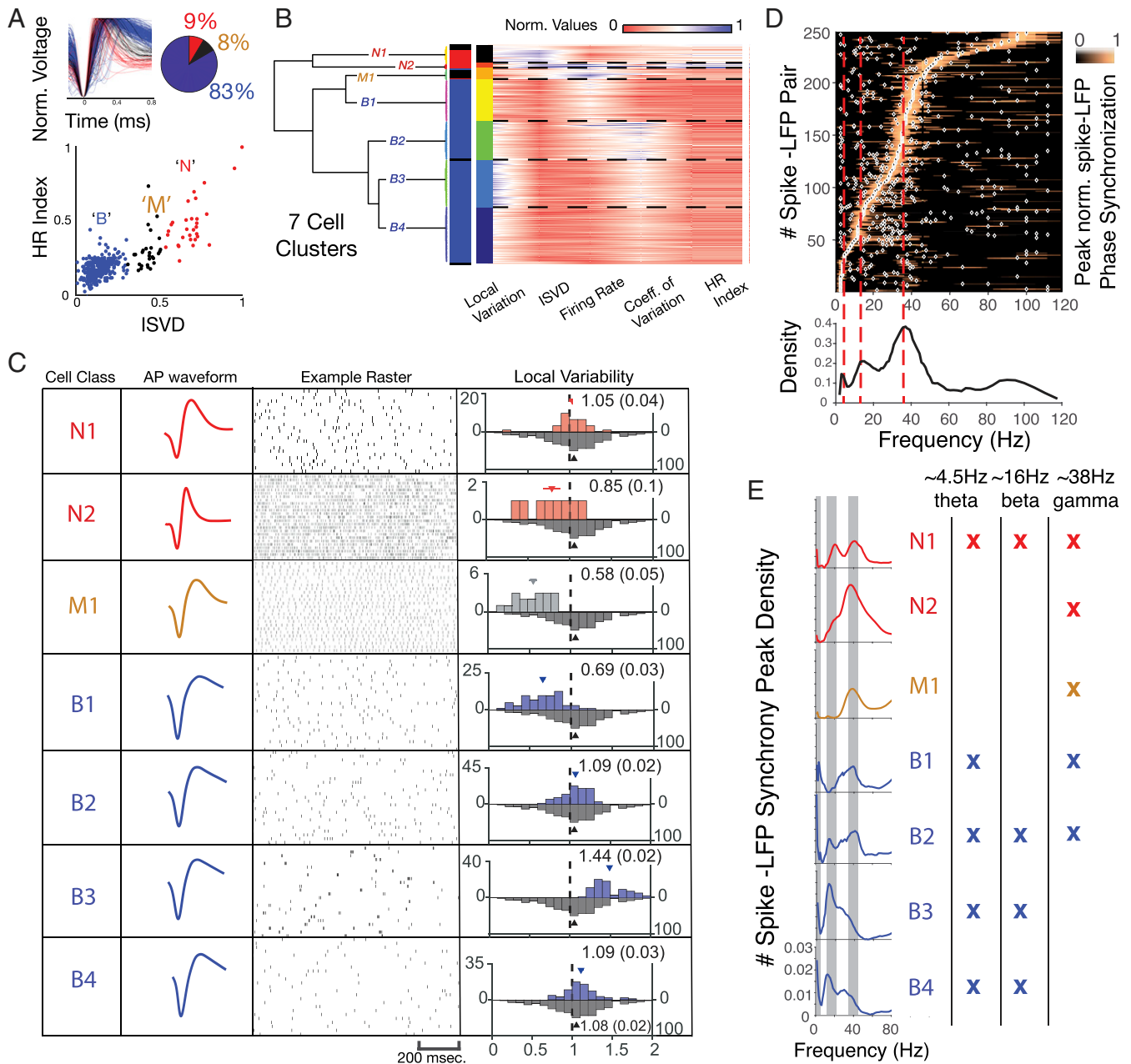
Fig. 2. Distinguishing striatal interneurons and projection neurons. (*A*) Normalized, average action potentials (APs) of striatal cells, color coded into 85% broad (B), 6% intermediate narrow (M), and 9% narrow (N) spiking neurons. These three AP classes are distinguished by their initial slope to valley decay (ISVD) and their hyperpolarization rate (HR) (*SI Appendix,* Fig. S1 *A–C*). (*B*) Dendogram showing the seven cell classes distinguishable with unsupervised *k*-means clustering taking into account the cell's ISVD, HR index, firing rate, local variability (LV), and coefficient of variation (CV). The clustering identifies four B classes (blue), two N classes (red), and one M class (orange) (*SI Appendix,* Fig. S1 *D–G*). (*C*) Example rasters, average AP waveforms, and distribution of LVs for each cell class. Three neuron classes showed highly regular interspike interval distributions (N2, M, and B1), B3 showed high burst firing propensity, and the other three classes (N1, B2, and B4) showed low firing rates and variable CVs (*SI Appendix,* Fig, S1*H*). (*D*) Peak normalized spike-to-local field potential (LFP) synchronization for all cells (*y* axis) across frequencies (*x* axis). Synchrony peaks across cells occurred around 4.5-Hz (theta), 16-Hz (low beta), and 38-Hz (gamma). White dots indicate significant (*P* < 0.05) synchrony peaks. (*E*) Density of significant synchrony peaks shows that theta and beta synchrony was more likely in broad spiking cell classes, while gamma band synchrony was apparent for narrow spiking classes N1, N2, and M1, as well as for broad spiking classes B1 and B2 (*SI Appendix,* Fig. S2).

broad spiking neurons) (Fig. 4*C*). In contrast, CP and EV were equally likely significantly correlated with the firing of narrow or broad spiking neurons (narrow/broad spiking neuron percentages with significant correlations of rate and CP: 23/18%; for rate and EV: 19/23%). These findings quantify that striatal FSI firing to the attention cue is more closely correlated with an internal state of confidence about the behaviorally relevant color

feature, than with the value or the actual choice probability of a stimulus.

Neural Responses to Go Cues and No-Go Cues. The firing changes to the attention cue could reflect the facilitation of processing the rewarded target stimulus or the suppression of the nonrewarded distracting stimulus. To disentangle these scenarios, we compared

Banaie Boroujeni et al.

www.manaraa.com
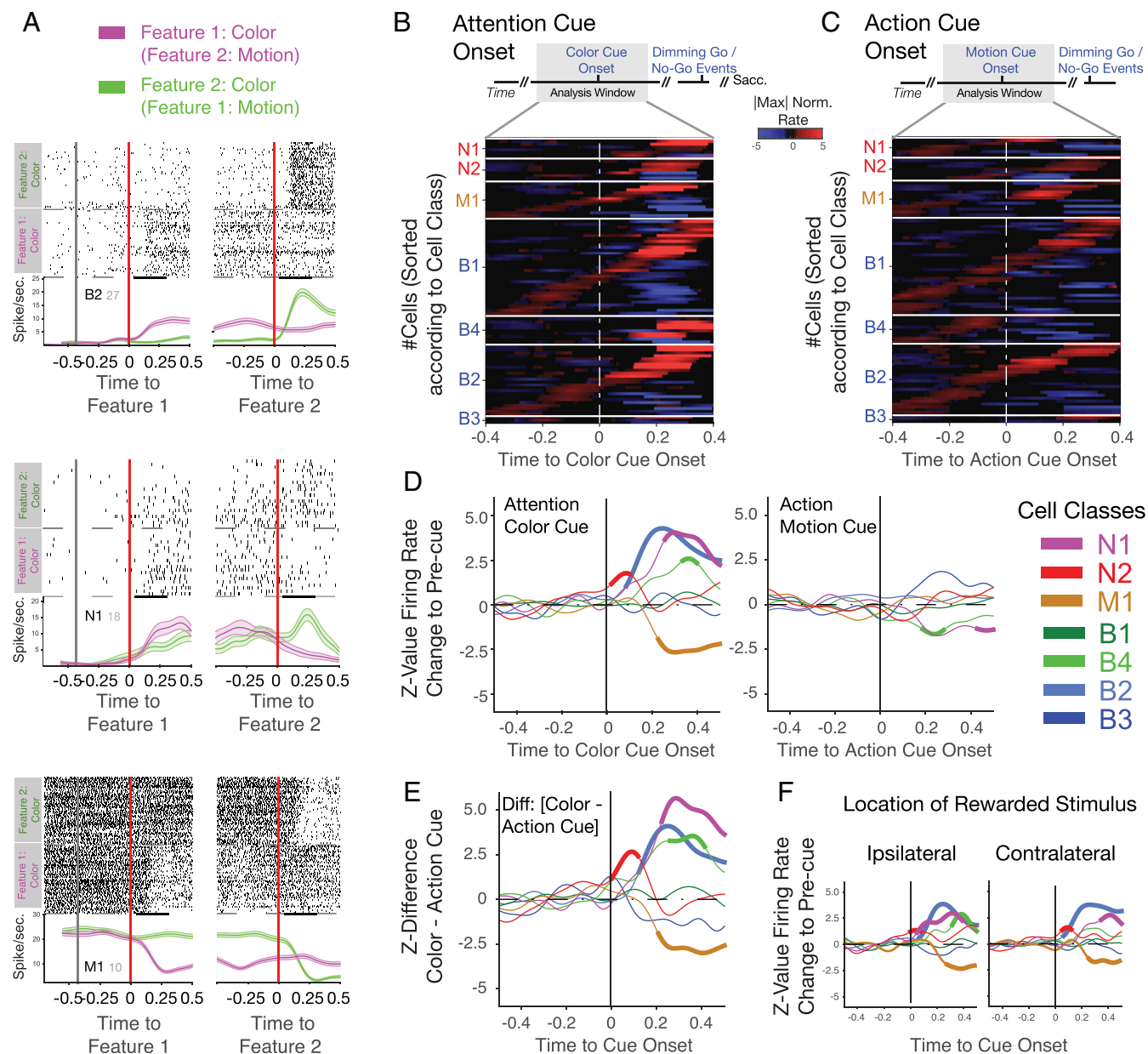
Fig. 3. Cell-class-specific firing rate changes to the attention color cue onset. (*A*) Three example cells with spike rasters around onset of the first cue (*Left*) and second cue (*Right*). The cells changed firing selectively when the attention color cue was onset either as first cue in the trial (purple), or as second cue (green). They showed no, or less, modulation to the action cue onset. Examples are from classes B2, N1, and M1. (*B*) Striatal cells (*y* axis) responded to the attention cue onset (0s on *x* axis) as shown by normalizing firing to the maximal or minimal firing around the time of attention cue onset. (*C*) There were fewer neurons responding to the action cue onset compared to *B*. (*D*) Z-normalized, average firing (thickened line denotes significance at $P < 0.05$) around the attention color cue onset (*Left*) shows that classes N1, N2, B2, and B4 showed periods with significant firing increase to the attention cue, while class M1 shows on average suppressed firing. There was markedly lower average modulation to the action cue (*Right*). Only N1 and B4 had brief periods of significantly suppressed action cue firing. (*E*) The difference of firing to the attention color cue versus action cue across cell classes. Thick lines indicate significance ($P < 0.05$, randomization test). (*F*) Z-normalized firing rate around color cue onset for correctly performed trials with the rewarded (target) color in the ipsilateral (*Left*) or the contralateral (*Right*) visual hemifield.

the responses of neurons to the transient dimming events that occurred in the rewarded target stimulus (go event, instructing a saccadic choice), and in the nonrewarded distractor stimulus (no-go event, instructing to ignore the event). We found that neurons in five of seven cell classes (N2, M1, B1, B2, and B4) showed on average significant response modulations to the go event (for four example cells and the Z-normalized average response, see *SI Appendix*, Fig. S5 *A* and *B*). However, we likewise found that three cell classes (M1, B3, and B4) on average significantly increased activity

to the no-go distractor event, indicating that subsets of cells increased their firing to a salient distractor event that needed to be suppressed (*SI Appendix*, Fig. S5*C*). These findings show that both facilitation of processing the relevant cues and suppressing the processing of salient distractors are represented in cell-class-specific firing increases. Statistically, the responses to the attended stimulus that indicate facilitation of its processing were stronger than the responses to the distracting events in the nonattended stimulus that indicate suppressing its influence on behavior (*SI Appendix*, Fig.

Banaie Boroujeni et al.

www.manaraa.com
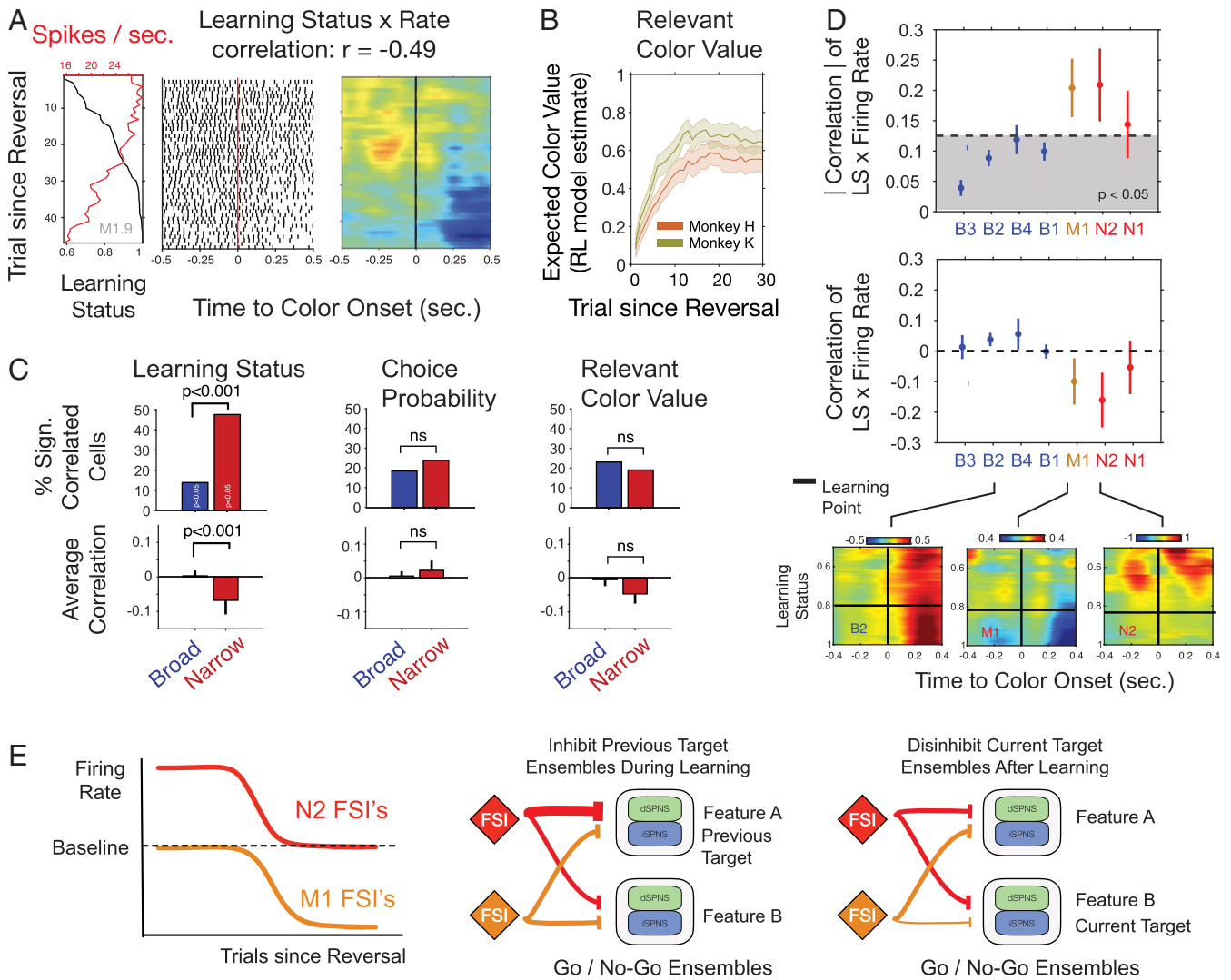
Fig. 4. Attention cue onset responses change with behavioral learning. (*A*) Example cell shows gradually reduced firing (red axis, *Left*) with increased probability of rewarded choices (learning status, black axis). Spike raster (*Middle*) and firing rate heat map (*Right*) illustrate that this cell shows negative rate x learning correlations ($r = -0.49$, $P < 0.01$). (*B*) Expected (Q) value of the rewarded color for trials since color-reward reversal as estimated by a feature-based reinforcement learning model. (*C*) Partial correlations of learning status (*Left*), choice probability (*Middle*), and expected value of the rewarded color (*Right*) for broad and narrow spiking cell classes. Panels show the proportion of significant correlations (*Upper* row) and the average correlation (*Lower* row). (*D*) Absolute (*Upper*) and signed (*Lower*) correlations of learning status (probability of rewarded choices) and Z-normalized firing rates in the attention cue epoch across cell classes. Gray shaded area denotes correlation range expected irrespective of cell class label (randomization test). Color panels (*Bottom*) show average learning x rate correlations for classes B2, M1, and N2. (*E*) Proposed interpretation of main results. N2 FSIs (red) are active during the reversal (*Left*) which could indicate inhibition of SPN ensembles encoding the previously relevant, now irrelevant feature (*Middle*). M1 FSIs (orange) are suppressed after learning, which could reflect reduced inhibition of those SPN cells that encode the currently relevant target feature (*Right*). Each feature-selective ensemble contains direct (green) and indirect (blue) pathway SPNs that cooperate to trigger facilitation (go) for that feature and a suppression (no-go) of competing features.

S5*D*). These response modulations to the go and no-go events changed with behavioral learning progress for classes M1 and B4 (Pearson correlations, $P < 0.01$, multiple comparison corrected, *SI Appendix*, Fig. S5*E*). For class M1 the firing rate changes to the go and no-go responses correlated on a trial-by-trial basis with the firing rate changes to the attention color cue (Dunn's test, $P < 0.05$). These findings indicate that the FSIs of the M1 class facilitate the processing of events not only when they directed covert attention (to the color onset), but also when they trigger an overt (saccadic) choice behavior (to the go event).

Spike-LFP Synchronization and LFP Power Change with Reversal Learning. So far, we have shown that the fast spiking neuron classes increased firing during learning (N2) or reduced firing

after learning (M1). These changes could be accompanied by changes in synchronization within the local circuit. We tested this for neurons that showed sufficient (≥ 40 spikes) spike activity in the 0.5 s following the attention cue onset by quantifying their spike-LFP phase synchronization. We found that fast spiking neurons (classes N2 and M1) did not alter their gamma band synchrony with learning, but showed on average increased 25- to 35-Hz beta band spike-LFP synchronization after learning was complete and performance reached asymptote (increased pairwise phase consistency in the beta band: 0.009 [SE 0.003]; $P < 0.05$) (Fig. 5*A*; for two examples, see *SI Appendix*, Fig. S6*A*). In contrast, broad spiking neurons (classes B1 to B4) showed on average significantly larger spike-LFP synchronization in a 45- to 55-Hz gamma band during learning than after learning, but no

www.manaraa.com

changes in synchrony in the beta band (increased pairwise phase consistency in the gamma band: −0.025 [SE 0.013]; $P < 0.05$) (Fig. 5A; for two examples see *SI Appendix*, Fig. S6A). These changes of the spike-LFP relationship were not a mere reflection of changes of LFP power (*SI Appendix*, Fig. S6B). LFP at recording sites with narrow spiking neurons showed significantly larger 15- to 25-Hz beta band power during learning and after learning showed significantly enhanced 35- to 40-Hz gamma band power ($n = 24$ LFP sites, $P < 0.05$ randomization test). LFP at recording sites with broad spiking neurons showed significantly increased theta band LFP power but no changes in beta and gamma bands ($n = 173$ LFP sites, $P < 0.05$ randomization test) (Fig. 5B).

Discussion

We found that striatal cells with a fast spiking firing pattern, narrow action potentials, and preferential synchrony to gamma band frequencies 1) responded stronger to attention cues than action cues and 2) negatively correlated with learning the reward prediction conveyed by attention cues. The correlations of neural cue responses and the behavioral learning progress of these fast spiking interneurons distinguished them from other cell types. Narrow spiking cells of the class N1 that were unlikely fast spiking cells increased firing to the attention cue but showed no consistent learning correlations. The four distinguishable classes of broad spiking cells were more heterogeneous in their cue responses and learning correlations. Across all cell types, the attention cue responses were more likely reflecting the facilitation of the attended target than the suppression of a nonattended distractor because the same cell types that responded to the cue also responded to the onset of the go event in the target stimuli. We found, however, three cell types that were on average responding to the salient no-go event (the transient dimming) of the distractor stimulus which suggests that their increased firing rate could reflect the suppression of processing distracting events. Finally, we found reversal learning did not alter the cell-class-specific gamma synchrony of fast spiking neurons or the beta synchrony of broad spiking neurons. Rather, gamma synchronous fast spiking neurons showed a increase in beta synchrony after learning, while beta synchronous broad spiking cell classes showed gamma synchrony during the period of reversal learning.

Taken together, these results show that there are two subclasses of striatal fast spiking neurons whose activity to an attention cue changes when the reward association of the attention cue is learned following reward reversals. One FSI class (N2) was particularly active during learning, signifying stronger inhibition during learning, while another FSI class (M1) became inactive after learning, signifying postlearning disinhibition of connected cells. These findings suggest that fast spiking interneurons in nonhuman primate striatum play a role in attention and learning processes that indexes cognitive flexibility.

Fast Spiking Interneuron Types Show Functional Specializations. Our key result is based on distinguishing two separate FSI classes (N2 and M1) that both contained neurons with repetitive firing pattern (low local variability), relatively high baseline firing rates, low global variability (coefficient of variation), and gamma rhythmic activity in vivo (34, 35, 42, 43). One FSI class (N2) showed the narrowest waveforms, while cells of the M1 class showed a rise and decay of their action potentials that was in between the narrow and the large broad spiking class. These unique spike dynamics indicate different underlying channel kinetics, suggesting these cell classes have different genetic fingerprints. A distinction of two subtypes of FSIs has recently been reported in rodent striatum when characterizing their morphology (35, 44) and when evaluating their activity profiles (36, 45). The finer-grained distinction of two FSI subtypes is not commonly reported in the literature, which might be because the distinct FSI subtypes both express parvalbumin (PV) (46) and might therefore be subsumed as PV^+ neurons without reporting further their action potential profiles (47).

Here, we found that two FSI cell types (N2 and M1) have not only different waveforms but show on average opposite functional firing characteristics. N2 neurons showed enhanced short, transient onset responses to the attention cue that were stronger during as compared to after learning (Figs. 3 and 4). In contrast, M1 cells showed decreased firing following cue onset that was more pronounced after subjects reached plateau performance (Fig. 4E). These differences suggest that N2 and M1 neurons play different roles in the local striatal circuit. Current anatomical insights into the specific roles of different FSIs are sparse (9, 48), but a recent study documented in mice and monkey striatum that two molecularly distinct FSI subtypes show different connectivity to SPNs linked to the direct and indirect pathway (46). One FSI subtype connects more strongly to SPN neurons whose activity is linked to the direct pathway that realizes a facilitation of cortical inputs and has been called the "go pathway" (3). We hypothesize that this FSI neuron subtype corresponds to the N2 class whose activity during learning might indicate the active inhibition of direct pathway SPNs that would otherwise facilitate the processing of the previously relevant target stimulus and thus needs to be inhibited during the reversal (Fig. 4 E, *Middle*). A possible mechanism for the enhanced FSI-mediated inhibition of SPNs during learning could be cortical input-induced short-term facilitation on FSIs (49) to enhance cortico-striatal feedforward inhibition onto those SPNs that should be prevented from responding to the previously relevant stimulus during the reversal learning (8, 13, 44).

We found that the other (M1) FSI class was suppressed below its baseline firing after learning of the new target feature occurred (Fig. 4 E, *Left*) and activated to the salient no-go event of the distractor stimulus with the irrelevant feature (*SI Appendix*, Fig. S5). We hypothesize that this FSI subtype will have connectivity for releasing inhibition of ensembles of SPNs encoding the newly relevant feature (Fig. 4 E, *Right*). Mechanistically, the reduced firing of M1 FSIs might not depend on cortical inputs. Rather the reduced firing of neurons in the M1 class might be mediated by thalamic-striatal inputs which have been reported to inhibit striatal FSIs (50) as well as to induce short-term depression on FSIs (49). The source of this thalamic inhibition of FSIs has been found in the thalamic reticular nucleus (50) whose neurons are known to activate during attention shifts (51) and whose integrity is necessary for attentional orienting (52). The
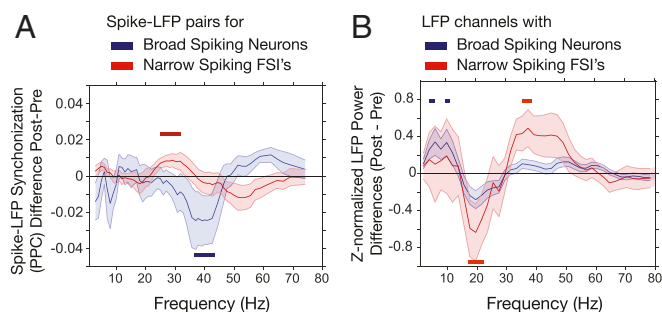
Fig. 5. Spike-LFP synchronization and LFP power change with behavioral learning. (A) Difference of spike-LFP synchronization (measured as pairwise phase consistency) after the learning criterion was reached versus before reaching criterion. Horizontal bars indicate significance at $P < 0.05$. Fast spiking interneurons (red) show increased 30-Hz synchrony after learning, while broad spiking neurons show decreased 40-Hz synchrony after learning. (B) Z-normalized LFP power from trials after versus before the learning criterion was reached. LFP channels were sorted into those with fast spiking interneuron activity (red) or broad spiking neuron activity (blue). Spike-LFP synchrony and power was calculated in a 500-ms window after the attention cue onset.

Banaie Boroujeni et al.

NEUROSCIENCE

striatal FSIs receiving this attention-charged input are thus expected to be inhibited when attention cues direct covert attention to a reward-associated location. Consistent with this scenario, the M1 FSI class could thus be the target for these thalamic inputs and hence support attention shifts to learned features through disinhibition of SPNs.

Taken together, the differential activation dynamics of the two FSI subclasses with learning suggests that the reversal learning of attention cues involves two stages that are mediated by functionally specialized striatal FSI circuits. We illustrate this hypothetical model in Fig. 4E. It assumes that in a first stage, one subtype of FSIs (containing N2 cells) is activated to inhibit SPNs encoding previously relevant target features and thereby suppress the now irrelevant inputs. In a second stage, a separate FSI subtype (containing M1 cells) receives thalamic inhibitory inputs that release those SPN ensembles from inhibition that encode the now relevant target features. The proposed two-stage process of adjusting attention sets during learning is constrained largely by rodent connectivity studies (with one exception) (46). The rodent cell types and cell-type-specific connectivities are likely only partly preserved in nonhuman primates (53). In light of this limitation, we believe that the two-stage hypothesis of cell-type-specific learning of attention provides important predictions for future studies dissecting the neural circuits underlying the learning of attention cues (23, 54, 55).

Beyond FSIs: Contributions of Spiny Projection Neurons, Low Threshold Interneurons, and Cholinergic Interneurons to the Learning of Attention. Our electrophysiological characterization of cell classes in the primate striatum did not only reveal two distinct classes of fast spiking interneurons but also five other distinguishable cell classes. One class was not fast spiking but had narrow action potential shapes (class N1), and four cell classes had broad action potentials (classes B1 to B4). Prior rodent studies have shown that broad and nonfast spiking striatal neurons are involved in reward learning and stimulus selection (3, 56), making it pivotal to discuss their putative involvement in our study. The nonfast spiking cell classes (N1 and B1 to B4) showed more heterogeneous response profiles to attention cues and correlations with learning compared to the FSI classes, suggesting that our electrophysiological classification and task paradigm is not sufficient to infer their circuit functions. These cell classes will encompass to different degrees SPNs, LTS interneurons, and cholinergic interneurons (CINs) as defined largely in rodents based on their unique morphology, protein expression, and in vitro physiology (6, 57). We believe there is evidence that links SPNs to neurons in classes B2 to B4, LTS interneurons to neurons in class N1, and CINs to neurons in B1. In particular, SPNs that constitute ~90% of striatal cells will be represented by neurons in classes B2 to B4 because of their broad waveforms, their spontaneous, irregular bursty firing patterns (58), and their beta band spike-LFP synchrony. The cell class specificity of beta band synchrony is consistent with prior studies that document how beta band synchrony among the SPN neural population can reflect how biased competition of cortical inputs to SPNs is resolved in favor of the more behaviorally relevant among competing inputs (59, 60). The only broad spiking cell class that did not show beta synchrony was cell class B1, whose tonic (and low) firing (lowest global and local variability, *SI Appendix*, Fig. S1H) suggest they encompass CINs (36, 61, 62). Subgroups of CINs have been shown to increase responding with reward learning (63), with CIN activation imposing a gain on reward learning (3), but their response patterns are heterogeneous and task-state dependent (64). This variability might explain why the B1 class did not show consistent functional correlations with learning in our task and suggests that understanding their circuit functions might require the use of more than one task paradigm. A similar conclusion applies to the class of inhibitory LTS cells, which are also tonically active neurons

(TANs), but which have narrower action potential waveforms, brief hyperpolarization, variable (regular to bursty) tonic firing (6, 35, 65), and low-frequency 3-7 Hz membrane oscillations (66). These characteristics of LTS neurons resemble neurons of our N1 class. This class showed strong attention cue responses, and apparent learning correlations consistent with a recent rodent study (56), but their overall correlational pattern was more variable than those of FSIs. We believe that narrowing down their circuit function will be possible with our electrophysiological profiling of cell classes, but will depend on a denser sampling of cells across the striatum (67).

The Anterior Striatum and Biasing of Selective Attention to Visual Features. Our study found that fast spiking interneurons, as well as neurons from three other classes modulated their activity stronger to the onset of a visual attention cue (the coloring of the two stimuli) than to visual cues carrying motor information (the motion direction of the stimuli) or to transient visual events that directly triggered an overt choice (the dimming of stimuli that served as a potential go-signal). This finding suggests that neurons in the anterior striatum play a role in covertly shifting attention. Consistent with such a role in attention, recent studies have shown that neural activity in the striatum indicates sustained covert spatial attention (26), the learning of feature-based attentional top-down control (23), and the covert selection of visual stimuli based on their expected value (25). The response modulations in these studies could reflect that neurons encode the expected reward value of specific visual features, or they might be more directly related to the actual choice probability with which one stimulus is chosen over another stimulus. We quantified these different possibilities by estimating the expected value and the choice probability of the chosen stimuli using an established reinforcement learning model (23, 33, 41, 68, 69). On average 18 to 23% of striatal neurons were significantly correlated with the expected value of the target stimulus, as well as with the choice probability of the chosen stimulus feature (Fig. 4C). This finding provides empirical support for an involvement of the striatum in both, valuation and a "covert choice" of attended visual features. However, the fast spiking interneuron population that varied their firing with the learning progress of the animals showed the strongest partial correlations not with stimulus values or choice probabilities, but with the subjects' confidence about the reward value of stimuli. This finding suggests that these neurons are not signaling the attention shift directly but indirectly as a decision variable that biases visual attention to prioritize processing one stimulus over another (70). It will be an important future task to characterize the specific information conveyed by striatal cell classes when attention is deployed during and after learning the value of stimulus features.

Taken together, the observed findings are an important step for understanding how subclasses of striatal cells contribute to flexibly reconfigure attentional priorities during learning and how reinforcement learning mechanisms shape the expression of learned attention (70, 71).

Materials and Methods

Electrophysiological recordings were made and anatomically reconstructed in two male rhesus macaques (*Macaca mulatta*) from the head of the caudate and the ventral striatum as described previously (23) (*SI Appendix*). For each single isolated neuron, we extracted the average action potential, mean firing rate (FR), Fano factor (FF, variance over mean of the spike count in consecutive time windows of 100 ms), the CV (SD over mean of the interspike intervals, as well as the LV) which is proportional to the square of the difference of two consecutive interspike intervals (37) (*SI Appendix*). We tested whether neurons fell into separate groups according to their action potential dynamics and firing statistics using a data driven *k*-means clustering technique and statistical approach as outlined previously (72) (*SI Appendix*).

To characterize the behavioral reversal learning status of the animals, we used an ideal observer statistic that determined the trial during a block when

the monkey showed consistent above-chance choices of the rewarded color as developed (40) and applied previously (41, 68) (*SI Appendix*). We estimated the choice probability and expected value of color for each trial relative to the reward reversal by cross-validating an attention-augmented reinforcement learning model that we previously validated against other models (23, 41, 68) (*SI Appendix*).

For spike-LFP analysis, we preprocessed the wideband data with the adaptive spike removal (ASR) method to remove spike bleed through artifacts as described in ref. 73 and calculated the pairwise phase consistency (PPC) with subsequent permutation testing to estimate significant spike-LFP synchronization (74) (*SI Appendix*).

1. O. Hikosaka *et al.*, Direct and indirect pathways for choosing objects and actions. *Eur. J. Neurosci.* **49**, 637–645 (2019).
2. S. I. Rusu, C. M. A. Pennartz, Learning, memory and consolidation mechanisms for behavioral control in hierarchically organized cortico-basal ganglia systems. *Hippocampus* **30**, 73–98 (2019).
3. J. Cox, I. B. Witten, Striatal circuits for reward learning and decision-making. *Nat. Rev. Neurosci.* **20**, 482–494 (2019).
4. S. Shipp, The functional logic of corticostriatal connections. *Brain Struct. Funct.* **222**, 669–706 (2017).
5. S. N. Haber, B. Knutson, The reward circuit: Linking primate anatomy and human imaging. *Neuropsychopharmacology* **35**, 4–26 (2010).
6. J. M. Tepper *et al.*, Heterogeneity and diversity of striatal GABAergic interneurons: Update 2018. *Front. Neuroanat.* **12**, 91 (2018).
7. J. D. Berke, Functional properties of striatal fast-spiking interneurons. *Front. Syst. Neurosci.* **5**, 45 (2011).
8. G. Silberberg, J. P. Bolam, Local and afferent synaptic pathways in the striatal microcircuitry. *Curr. Opin. Neurobiol.* **33**, 182–187 (2015).
9. M. Assous, D. Dautan, J. M. Tepper, J. Mena-Segovia, Pedunculopontine glutamatergic neurons provide a novel source of feedforward inhibition in the striatum by selectively targeting interneurons. *J. Neurosci.* **39**, 4727–4737 (2019).
10. S. R. Lapper, Y. Smith, A. F. Sadikot, A. Parent, J. P. Bolam, Cortical input to parvalbumin-immunoreactive neurones in the putamen of the squirrel monkey. *Brain Res.* **580**, 215–224 (1992).
11. B. D. Bennett, J. P. Bolam, Synaptic input and output of parvalbumin-immunoreactive neurons in the neostriatum of the rat. *Neuroscience* **62**, 707–719 (1994).
12. D. A. Burke, H. G. Rotstein, V. A. Alvarez, Striatal local circuitry: A new framework for lateral inhibition. *Neuron* **96**, 267–284 (2017).
13. J. J. Belić, A. Kumar, J. Hellgren Kotaleski, Interplay between periodic stimulation and GABAergic inhibition in striatal network oscillations. *PLoS One* **12**, e0175135 (2017).
14. S. F. Owen, J. D. Berke, A. C. Kreitzer, Fast-spiking interneurons supply feedforward control of bursting, calcium, and plasticity for efficient learning. *Cell* **172**, 683–695.e15 (2018).
15. K. Lee *et al.*, Parvalbumin interneurons modulate striatal output and enhance performance during associative learning. *Neuron* **93**, 1451–1463.e4 (2017).
16. L. Carrillo-Reid *et al.*, Encoding network states by striatal cell assemblies. *J. Neurophysiol.* **99**, 1435–1450 (2008).
17. E. G. Antzoulatos, E. K. Miller, Differences between neural activity in prefrontal cortex and striatum during learning of novel abstract categories. *Neuron* **71**, 243–249 (2011).
18. R. Kawagoe, Y. Takikawa, O. Hikosaka, Expectation of reward modulates cognitive signals in the basal ganglia. *Nat. Neurosci.* **1**, 411–416 (1998).
19. M. S. Jog, Y. Kubota, C. I. Connolly, V. Hillegaart, A. M. Graybiel, Building neural representations of habits. *Science* **286**, 1745–1749 (1999).
20. J. R. Hollerman, L. Tremblay, W. Schultz, Influence of reward expectation on behavior-related neuronal activity in primate striatum. *J. Neurophysiol.* **80**, 947–963 (1998).
21. F. Hadj-Bouziane, D. Boussaoud, Neuronal activity in the monkey striatum during conditional visuomotor learning. *Exp. Brain Res.* **153**, 190–196 (2003).
22. A. Pasupathy, E. K. Miller, Different time courses of learning-related activity in the prefrontal cortex and striatum. *Nature* **433**, 873–876 (2005).
23. M. Oemisch *et al.*, Feature-specific prediction errors and surprise across macaque fronto-striatal circuits. *Nat. Commun.* **10**, 176 (2019).
24. B. Lau, P. W. Glimcher, Value representations in the primate striatum during matching behavior. *Neuron* **58**, 451–463 (2008).
25. S. R. Santacruz, E. L. Rich, J. D. Wallis, J. M. Carmena, Caudate microstimulation increases value of specific choices. *Curr. Biol.* **27**, 3375–3383.e3 (2017).
26. F. Arcizet, J. R. Krauzlis, Covert spatial selection in primate basal ganglia. *PLoS Biol.* **16**, e2005930 (2018).
27. Z. M. Williams, E. N. Eskandar, Selective enhancement of associative learning by microstimulation of the anterior caudate. *Nat. Neurosci.* **9**, 562–568 (2006).
28. K. Nakamura, O. Hikosaka, Facilitation of saccadic eye movements by postsaccadic electrical stimulation in the primate caudate. *J. Neurosci.* **26**, 12885–12895 (2006).
29. K. I. Amemori, S. Amemori, D. J. Gibson, A. M. Graybiel, Striatal microstimulation induces persistent and repetitive negative decision-making predicted by striatal beta-band oscillation. *Neuron* **99**, 829–841.e6 (2018).
30. S. Nonomura *et al.*, Monitoring and updating of action selection for goal-directed behavior through the striatal direct and indirect pathways. *Neuron* **99**, 1302–1314.e5 (2018).
31. L. H. Tai, A. M. Lee, N. Benavidez, A. Bonci, L. Wilbrecht, Transient stimulation of distinct subpopulations of striatal neurons mimics changes in action value. *Nat. Neurosci.* **15**, 1281–1289 (2012).
32. P. Znamenskiy, A. M. Zador, Corticostriatal neurons in auditory cortex drive decisions during auditory discrimination. *Nature* **497**, 482–485 (2013).
33. Y. Niv *et al.*, Reinforcement learning in multidimensional environments relies on attention mechanisms. *J. Neurosci.* **35**, 8145–8157 (2015).
34. J. D. Berke, Fast oscillations in cortical-striatal networks switch frequency following rewarding events and stimulant drugs. *Eur. J. Neurosci.* **30**, 848–859 (2009).
35. Y. Kawaguchi, Physiological, morphological, and histochemical characterization of three classes of interneurons in rat neostriatum. *J. Neurosci.* **13**, 4908–4923 (1993).
36. A. Sharott *et al.*, Different subtypes of striatal neurons are selectively modulated by cortical oscillations. *J. Neurosci.* **29**, 4571–4585 (2009).
37. S. Shinomoto *et al.*, Relating neuronal firing patterns to functional differentiation of cerebral cortex. *PLOS Comput. Biol.* **5**, e1000433 (2009).
38. M. A. van der Meer *et al.*, Integrating early results on ventral striatal gamma oscillations in the rat. *Front. Neurosci.* **4**, 300 (2010).
39. M. W. Howe, H. E. Atallah, A. McCool, D. J. Gibson, A. M. Graybiel, Habit learning is associated with major shifts in frequencies of oscillatory activity and synchronized spike firing in striatum. *Proc. Natl. Acad. Sci. U.S.A.* **108**, 16801–16806 (2011).
40. A. C. Smith *et al.*, Dynamic analysis of learning in behavioral experiments. *J. Neurosci.* **24**, 447–461 (2004).
41. S. A. Hassani *et al.*, A computational psychiatry approach identifies how alpha-2A noradrenergic agonist Guanfacine affects feature-based reinforcement learning in the macaque. *Sci. Rep.* **7**, 40606 (2017).
42. G. Sciamanna, C. J. Wilson, The ionic mechanism of gamma resonance in rat striatal fast-spiking neurons. *J. Neurophysiol.* **106**, 2936–2949 (2011).
43. G. J. Gage, C. R. Stoetzner, A. B. Wiltschko, J. D. Berke, Selective activation of striatal fast-spiking interneurons during choice execution. *Neuron* **67**, 466–479 (2010).
44. T. Koós, J. M. Tepper, Inhibitory control of neostriatal projection neurons by GABAergic interneurons. *Nat. Neurosci.* **2**, 467–472 (1999).
45. J. D. Berke, Uncoordinated firing rate changes of striatal fast-spiking interneurons during behavioral task performance. *J. Neurosci.* **28**, 10075–10080 (2008).
46. F. N. Garas *et al.*, Secretagogin expression delineates functionally-specialized populations of striatal parvalbumin-containing interneurons. *eLife* **5**, e16088 (2016).
47. T. Womelsdorf, Neocortical cell classes: Essential contributions from Electrophysiology. *Curr. Biol.* **29**, R871–R873 (2019).
48. M. Assous *et al.*, Differential processing of thalamic information via distinct striatal interneuron circuits. *Nat. Commun.* **8**, 15860 (2017).
49. G. Sciamanna, G. Ponterio, G. Mandolesi, P. Bonsi, A. Pisani, Optogenetic stimulation reveals distinct modulatory properties of thalamostriatal vs corticostriatal glutamatergic inputs to fast-spiking interneurons. *Sci. Rep.* **5**, 16742 (2015).
50. J. R. Klug *et al.*, Differential inputs to striatal cholinergic and parvalbumin interneurons imply functional distinctions. *eLife* **7**, e35657 (2018).
51. K. McAlonan, J. Cavanaugh, R. H. Wurtz, Attentional modulation of thalamic reticular neurons. *J. Neurosci.* **26**, 4444–4450 (2006).
52. G. D. Weese, J. M. Phillips, V. J. Brown, Attentional orienting is impaired by unilateral lesions of the thalamic reticular nucleus in the rat. *J. Neurosci.* **19**, 10135–10139 (1999).
53. R. D. Hodge *et al.*, Conserved cell types with divergent features in human versus mouse cortex. *Nature* **573**, 61–68 (2019).
54. A. Radulescu, Y. Niv, I. Ballard, Holistic reinforcement learning: The role of structure and attention. *Trends Cogn. Sci.* **23**, 278–292 (2019).
55. D. N. George, A. M. Duffaud, S. Killcross, "Neural correlates of attentional set" in *Attention and Associative Learning*, C. J. Mitchell, M. E. Le Pelley, Eds. (Oxford University Press, New York, 2010), pp. 351–384.
56. E. N. Holly *et al.*, Striatal low-threshold spiking interneurons regulate goal-directed learning. *Neuron* **103**, 92–101.e6 (2019).
57. M. Assous, J. M. Tepper, Excitatory extrinsic afferents to striatal interneurons and interactions with striatal microcircuitry. *Eur. J. Neurosci.* **49**, 593–603 (2019).
58. C. J. Wilson, P. M. Groves, Spontaneous firing patterns of identified spiny neurons in the rat neostriatum. *Brain Res.* **220**, 67–80 (1981).
59. S. Ardid *et al.*, Biased competition in the absence of input bias revealed through corticostriatal computation. *Proc. Natl. Acad. Sci. U.S.A.* **116**, 8564–8569 (2019).
60. E. G. Antzoulatos, E. K. Miller, Increases in functional connectivity between prefrontal cortex and striatum during category learning. *Neuron* **83**, 216–225 (2014).
61. J. A. Goldberg, C. J. Wilson, Control of spontaneous firing patterns by the selective coupling of calcium currents to calcium-activated potassium currents in striatal cholinergic interneurons. *J. Neurosci.* **25**, 10230–10238 (2005).

Banaie Boroujeni et al.

NEUROSCIENCE

www.manaraa.com

62. B. D. Bennett, J. C. Callaway, C. J. Wilson, Intrinsic membrane properties underlying spontaneous tonic firing in neostriatal cholinergic interneurons. *J. Neurosci.* **20**, 8493–8503 (2000).

63. T. Aosaki *et al.*, Responses of tonically active neurons in the primate's striatum undergo systematic changes during behavioral sensorimotor conditioning. *J. Neurosci.* **14**, 3969–3984 (1994).

64. P. Apicella, Leading tonically active neurons of the striatum from reward detection to context recognition. *Trends Neurosci.* **30**, 299–306 (2007).

65. J. A. Beatty, M. A. Sullivan, H. Morikawa, C. J. Wilson, Complex autonomous firing patterns of striatal low-threshold spike interneurons. *J. Neurophysiol.* **108**, 771–781 (2012).

66. S. C. Song, J. A. Beatty, C. J. Wilson, The ionic mechanism of membrane potential oscillations and membrane resonance in striatal LTS interneurons. *J. Neurophysiol.* **116**, 1752–1764 (2016).

67. E. Fino, M. Vandecasteele, S. Perez, F. Saudou, L. Venance, Region-specific and state-dependent action of striatal GABAergic interneurons. *Nat. Commun.* **9**, 3339 (2018).

68. M. Balcarras, S. Ardid, D. Kaping, S. Everling, T. Womelsdorf, Attentional selection can Be predicted by reinforcement learning of task-relevant stimulus features weighted by value-independent stickiness. *J. Cogn. Neurosci.* **28**, 333–349 (2016).

69. Y. C. Leong, A. Radulescu, R. Daniel, V. DeWoskin, Y. Niv, Dynamic interaction between reinforcement learning and attention in multidimensional environments. *Neuron* **93**, 451–463 (2017).

70. T. Womelsdorf, S. Everling, Long-range attention networks: Circuit motifs underlying endogenously controlled stimulus selection. *Trends Neurosci.* **38**, 682–700 (2015).

71. R. J. Krauzlis, A. Bollimunta, F. Arcizet, L. Wang, Attention as an effect not a cause. *Trends Cogn. Sci.* **18**, 457–464 (2014).

72. S. Ardid *et al.*, Mapping of functionally characterized cell classes onto canonical circuit operations in primate prefrontal cortex. *J. Neurosci.* **35**, 2975–2991 (2015).

73. K. Banaie Boroujeni, P. Tiesinga, T. Womelsdorf, Adaptive spike-artifact removal from local field potentials uncovers prominent beta and gamma band neuronal synchronization. *J. Neurosci. Methods* **330**, 108485 (2020).

74. M. Vinck, F. P. Battaglia, T. Womelsdorf, C. Pennartz, Improved measures of phase-coupling between spikes and the local field potential. *J. Comput. Neurosci.* **33**, 53–75 (2012).

Banaie Boroujeni et al.

www.manaraa.com